

Laboratory for  
Experimental  
Astrophysics

UCRL-JC-118213  
PREPRINT

*Integrated X-ray Testing of the Electro-  
Optical Breadboard Model for the XMM  
Reflection Grating Spectrometer*

J.V. Bixler,<sup>1</sup> H. Aarts,<sup>2</sup> W. Burkert,<sup>3</sup> T. den Boggende,<sup>2</sup>  
G. Branduardi-Raymont,<sup>4</sup> H. Brauninger,<sup>3</sup> A.C. Brinkman,<sup>2</sup>  
W. Craig,<sup>1</sup> T. Decker,<sup>1</sup> L. Dubbeldam,<sup>5</sup> C. Erd,<sup>6</sup> C.J. Hailey,<sup>1</sup>  
J.W. den Herder,<sup>5</sup> F.A. Jansen,<sup>5</sup> S.M. Kahn,<sup>1,7</sup> P.A.J. de Korte,<sup>2</sup>  
C.W. Mauche,<sup>1</sup> F.B.S. Paerels,<sup>7</sup> K. Thomsen<sup>8</sup>

1. Laboratory for Experimental Astrophysics, Lawrence Livermore  
National Laboratory; 2. Space Research Organization Netherlands,  
Utrecht; 3. Max-Planck Institute fur Extraterrestische Physik, Testanlage  
PANTER; 4. Mullard Space Science Laboratory, University College  
London; 5. Space Research Organization Netherlands, Leiden; 6. ESA  
Space Science Dept., ESTEC; 7. Dept. of Physics, University of California  
Berkeley; 8. Paul Scherrer Institut, Villigen

This paper was prepared for submittal to SPIE's 1994  
International Symposium on Optics, Imaging, and  
Instrumentation, July 24-29, 1994, San Diego, CA

MASTER

July 12, 1994

Lawrence Livermore National Laboratory • University of California

~~DISTRIBUTION~~ OF THIS DOCUMENT IS UNLIMITED



## DISCLAIMER

This document was prepared as an account of work sponsored by an agency of the United States Government. Neither the United States Government nor the University of California nor any of their employees, makes any warranty, express or implied, or assumes any legal liability or responsibility for the accuracy, completeness, or usefulness of any information, apparatus, product, or process disclosed, or represents that its use would not infringe privately owned rights. Reference herein to any specific commercial product, process, or service by trade name, trademark, manufacturer, or otherwise, does not necessarily constitute or imply its endorsement, recommendation, or favoring by the United States Government or the University of California. The views and opinions of authors expressed herein do not necessarily state or reflect those of the United States Government or the University of California, and shall not be used for advertising or product endorsement purposes.

This is a preprint of a paper intended for publication in a journal or proceedings. Since changes may be made before publication, this preprint is made available with the understanding that it will not be cited or reproduced without the permission of the author.

## **DISCLAIMER**

**Portions of this document may be illegible in electronic image products. Images are produced from the best available original document.**

# Integrated X-ray Testing of the Electro-Optical Breadboard Model for the XMM Reflection Grating Spectrometer

J. V. Bixler<sup>1</sup>, H. Aarts<sup>2</sup>, W. Burkert<sup>3</sup>, T. den Boggende<sup>2</sup>, G. Branduardi-Raymont<sup>4</sup>, H. Brauning<sup>3</sup>, A. C. Brinkman<sup>2</sup>, W. W. Craig<sup>1</sup>, T. Decker<sup>1</sup>, L. Dubbeldam<sup>5</sup>, C. Erd<sup>6</sup>, C. J. Hailey<sup>1</sup>, J. W. den Herder<sup>5</sup>, F. A. Jansen<sup>5</sup>, S. M. Kahn<sup>1,7</sup>, P. A. J. de Korte<sup>2</sup>, C. W. Mauche<sup>1</sup>, F. B. S. Paerels<sup>7</sup>, K. Thomsen<sup>8</sup>

1. Laboratory for Experimental Astrophysics, Lawrence Livermore National Laboratory, Livermore, CA 94550
2. Space Research Organization Netherlands, Sorbonnelaan 2, 3584 CA Utrecht, The Netherlands
3. Max-Planck-Institut für Extraterrestrische Physik, Testanlage PANTER, Gautingerstrasse 45, Fa., Pantolsky, 8027 Neuried b. München, Germany
4. Mullard Space Science Laboratory, Department of Physics and Astronomy, University College, London, Hombury St. Mary, Dorking, Surrey RH5 6NT, England
5. Space Research Organization Netherlands, Niels Bohrweg 2, 2333 AL Leiden, The Netherlands
6. ESA Space Science Department, ESTEC, Postbus 299, 2200AG Noordwijk, The Netherlands
7. Department of Physics, University of California, Berkeley, CA 94720
8. Paul Scherrer Institut, Villigen, CH-5232 Villigen PSI, Switzerland

## ABSTRACT

X-ray calibration of the Electro-Optical Breadboard Model (EOBB) of the XMM Reflection Grating Spectrometer has been carried out at the Panter test facility in Germany. The EOBB prototype optics consisted of a four-shell grazing incidence mirror module followed by an array of eight reflection gratings. The dispersed x-rays were detected by an array of three CCDs. Line profile and efficiency measurements were made at several energies, orders, and geometric configurations for individual gratings and for the grating array as a whole. The x-ray measurements verified that the grating mounting method would meet the stringent tolerances necessary for the flight instrument.

Post EOBB metrology of the individual gratings and their mountings confirmed the precision of the grating boxes' fabrication. Examination of the individual grating surface's at micron resolution revealed the cause of anomalously wide line profiles to be scattering due to the crazing of the replica's surface.

## 1. INTRODUCTION

The Reflection Grating Spectrometer (RGS) is part of the X-ray Multimirror Mission (XMM) satellite scheduled to launch in 1999<sup>1</sup>. The RGS will perform high-resolution spectroscopy between 0.35 - 2.5 keV (5 - 38 Å) with a resolving power of about 400 at 0.5 keV in first order. The spectral range selected for the RGS contains the K-shell transitions of the abundant light elements and the important L-shell transitions of Fe. The RGS resolving power is sufficient to measure the intensity of the three lines of the He-like triplets of the most abundant elements in the spectral band and will provide an important diagnostic capability for astrophysical plasmas.

In order to verify the performance of the RGS design concepts, the Electro-Optical Bread Board (EOBB) test was carried out at the Panter x-ray test facility in the fall of 1993. The test brought together prototype elements of the RGS for an integrated test of instrument efficiency and resolution. This test was the first integrated measure of RGS performance which, before delivery to the Panter facility, could only be inferred from the testing of the individual elements and by raytracing.

In addition to the initial verification of instrument performance, the tests provided experience to the RGS team in instrument alignment, planning and executing test procedures, and familiarization with the calibration facility. This experience will prove invaluable for future tests.

## 2. RGS OPTICAL CONFIGURATION

XMM will have three identical x-ray telescopes, two of which will have attached grating boxes and associated CCD detector strips. The optical layout for one of these spectrometers is shown in Figure 1. X-rays exiting the telescope are partially intercepted by the grating box and diffracted to the CCD detector strip. Forty-three percent of the light exiting the telescope will be intercepted by the gratings; forty percent passes through the grating box to be detected by the European Photon Imaging Camera (EPIC) at the focal plane and the remaining light is obscured by the grating box structure. The grating box, CCDs, and EPIC sit on a Rowland circle of diameter 6705.3 mm.

The three telescopes on the flight instrument will consist of 58 nested, coaxial, and confocal Wolter I mirror shells ranging in diameter from 306 mm to 700 mm. Shell thicknesses range from 0.4 mm for the inner shells to 1.2 mm for the outer shells. All mirror shells have an overall length of 600 mm and a 7.5 meter focal length. The shells are produced

**MASTER**

by electroforming nickel on diamond-turned and polished mandrels. A gold coating evaporated onto the mandrels before the nickel is deposited provides the reflecting surface.

For the EOB tests, mirror shells 1, 40, 41, and 58 (shell 1 being the largest diameter) were assembled into the Mirror Development Module (MDM). The four mirror shells were mounted into grooves on sixteen-finger spiders at both the front and back rims. The production, mounting, and performance of the initial mirror shells has been described by Citterio et al.<sup>2</sup>.

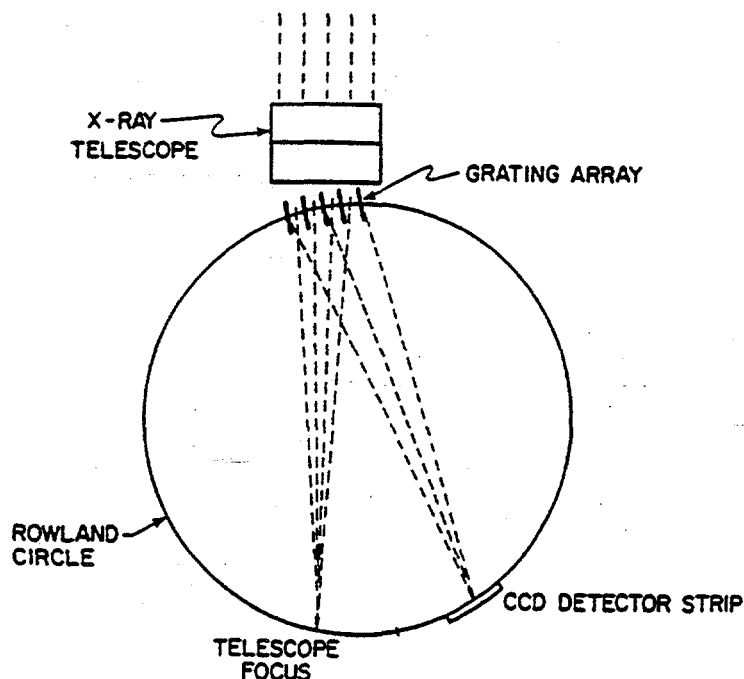


Figure 1. A schematic representation of the optical design of the RGS. An array of reflection gratings is oriented at grazing incidence to the beam exiting an x-ray telescope. The gratings intercept roughly half of the beam with the rest passing through to a focal plane detector. Rays which are intercepted are diffracted to a strip of CCDs which serve as the spectroscopic detector. The gratings, telescope focus, and the CCD detector strip all lie on a Rowland circle of 6705.3 mm diameter. The Rowland configuration eliminates aberrations associated with the arraying geometry.

The flight RGS grating array will contain about 200 gratings housed in a beryllium structure. The distance from the midpoint of the grating array to the telescope focus is designed to be exactly 6.7 meters. The grating centers sit on a toroidal surface produced by rotating the Rowland circle about a line which passes through the telescope focus and the  $\lambda = 15\text{\AA}$  first-order spectral focus. Each grating is slightly tilted with respect to its neighbor so that the incidence angle of the converging x-ray beam at the midpoint of each grating is 1.576 degrees.

For the EOB tests, the grating box contained eight gratings mounted in an Invar weldment structure. This structural material was a compromise chosen to be as stiff as possible while satisfying cost and scheduling constraints.

The eight diffraction gratings mounted in the grating box were produced through replication from a single master grating<sup>3,4</sup>. The individual gratings were replicated with a thin gold coated surface onto flight-like Silicon Carbide substrates approximately 200 mm by 100 mm in size and 1 mm thick. The substrates had integral stiffening ribs on the back side running in the long direction and were flat to within 0.7 wave of optical light in the long direction and 7 waves in the short direction. The gratings were held in place using diamond-turned bosses which contacted the grating at each corner. A full description of the grating box design, fabrication, and metrology is given in Decker et al.<sup>5</sup>

The gratings have a central line density of 645.6 lines per millimeter. The triangular facets are blazed at 0.7 degrees to produce peak efficiency at  $15\text{\AA}$  in first order. A variable line spacing of approximately  $\pm 3$  percent along the grating's length is necessary to produce a stigmatic diffraction spot for  $15\text{\AA}$  on the Rowland circle. Measurement of the replicated gratings' efficiency before the EOB tests are shown in Figure 2a. The replicated gratings retained 80 percent of the master's first order efficiency for both Cu L and Al K energies.

In the flight instrument the diffracted light from the grating box is intercepted by an array of nine CCDs which record the x-ray spectrum from 5 to 38  $\text{\AA}$ . The CCD's are designed to be edge buttable with minimal loss of detection area at the mating edges. Each CCD has a detection region and an image storage/readout section of 1024 by 384 pixels. Each pixel is 27 microns square. The CCDs are read out in frame transfer mode through two output registers. The typical readout time

of a pixel is 15  $\mu$ sec with 20  $\mu$ sec needed for a line shift. The total readout time for a frame taken during EOBB testing was 3.73 seconds.

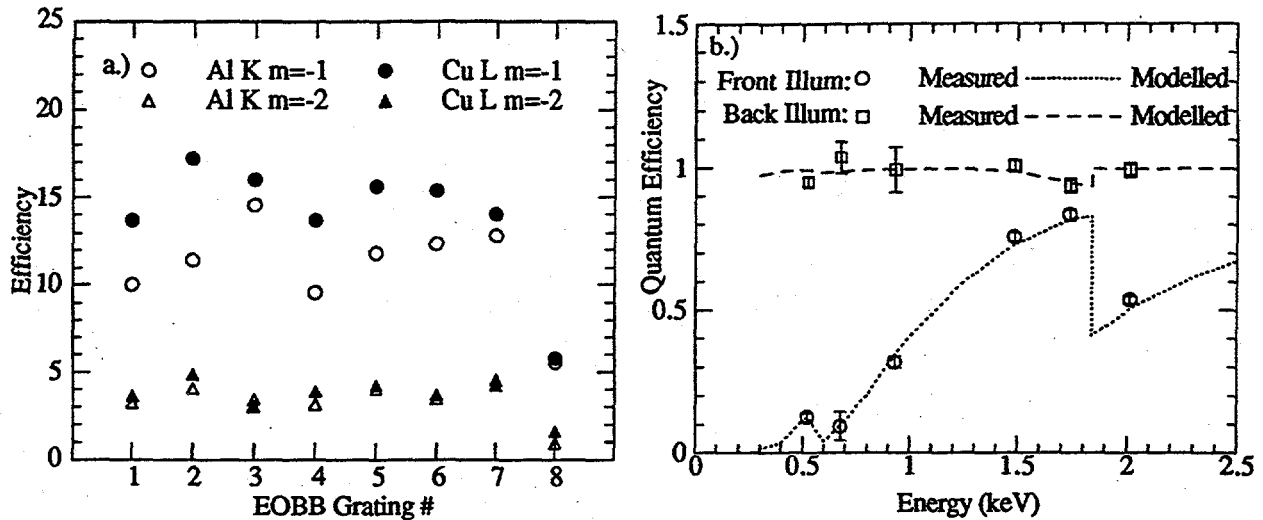


Figure 2. Pre EOBB measured efficiencies of RGS components a.) Efficiencies of the eight grating replicas used in the grating box. b.) Quantum efficiency for the front- and back-illuminated CCDs used in the focal plane detector.

In order to achieve high quantum efficiency at low energies, the baseline design for the flight focal plane camera employs thinned, back-illuminated CCDs. At the time of the EOBB tests only one back-illuminated device was available. For the EOBB focal plane camera, the back illuminated device was mounted in a prototype camera head with two front-illuminated devices. The laboratory measured efficiency of both types of devices is shown in Figure 2b. The superiority of the back illuminated device is clearly evident.

### 3. TEST CONFIGURATION

A top view of the Panter x-ray calibration facility as used in the EOBB tests is shown in Figure 3. The coordinate system used placed the origin at the telescope focus with positive x pointing away from the source, positive y opposite the gravity vector, and negative z in the dispersion direction.

The x-ray source is at the end of a 120 meter long evacuated tube connecting the source housing with the experiment chamber. The finite source distance displaced the telescope focal point 0.5 meters behind the nominal flight focal point. To account for this focal shift, and preserve the Rowland circle geometry, the grating box was moved 0.5 m further from the telescope than in the flight configuration.

An electron impact source employing several different anode materials produced the x-ray flux for all measurements. The incident electron beam was focused to a line source on the anode face. The line of emission was viewed at an angle to project a one mm spot size. Anodes used during the testing included Al, Mg, Cu, P, and  $\text{SiO}_2/\text{Cu}$ . Depending on the source, an Al, B or Nb thin film filter was used to reduce bremsstrahlung and optical light.

A monochromator was inserted when resolution measurements were taken with intrinsically broad (compared to the instrumental resolution of 400) L-shell lines. A Hettrick Surface Normal Rotation monochromator provided a spectral purity of  $E/\Delta E \approx 900$  using a 10  $\mu\text{m}$  exit slit.

The newly refurbished experiment chamber measured 12.8 m long by 3.6 m in diameter. At the throat of the chamber a proportional counter was used to monitor the source flux. The chamber contained two large platforms, one to hold the telescope and grating box, the other to hold the detectors. The telescope/grating box platform was capable of simulating off-axis angles by remotely tilting about the y and z axis on a ball joint mounted directly beneath the paraboloid/hyperboloid interface of the telescope.

The telescope was mounted on a fixture allowing rotation about the optical axis in ninety degree increments and translation in the z direction. The rotation allowed different sectors of the mirror to feed the grating box. A "curtain" assembly was placed in front of the telescope aperture which allowed the remote selection of different mirror shells for illumination by the source. For the EOBB tests, shell 58, shells 40/41 or all four available shells could be selected.

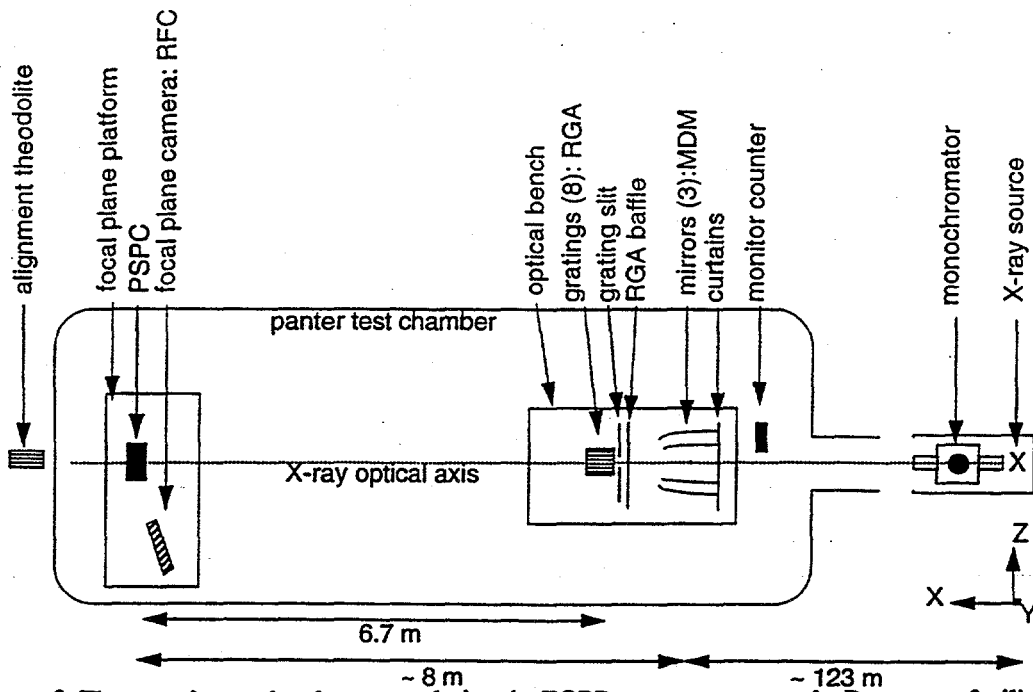


Figure 3. The experiment chamber set up during the EOB measurements at the Panter test facility.

The grating box assembly sat directly behind the MDM on a stack of three manipulators. Since the MDM area that could be covered by the eight grating box was relatively small, the box was designed to move to three different positions along the MDM's exiting beam as shown in Figure 4a. A baffle mounted between the mirror and the grating box limited the mirror illumination to the area covered by the grating box. The box was kinematically mounted on the manipulator stack using three gauge blocks which provided the correct Rowland torus orientation. The majority of the measurements were made in the "6 o'clock" position, shown in Figure 4b, with the grating box directly below the optical axis and intercepting x-rays from the three innermost mirror shells.

Measurements were also made at the "3 o'clock" position (which in reality was closer to 4 o'clock) with the grating box placed just below the x-z plane and translated in z to intercept x-rays from the three innermost shells. This second position allowed measurements to be made with the x-rays taking a markedly different optical path. The spot produced this way was visibly different from those produced at 6 o'clock and were extremely useful for raytrace comparisons.

The grating box was designed for use at the 6 o'clock position. To use the same box in the 3 o'clock position the Rowland circle was rotated around the origin so as to translate the grating box from the 6 o'clock to the 3 o'clock position. This was accomplished physically by repositioning and realigning the entire manipulator stack and moving the RFC to match the shift of the spectral focus.

The grating box manipulators allowed z and x translation and rotation about the y axis. These translations and rotations allowed the grating box to be presented to the converging x-ray beam in a variety of aligned and misaligned positions. The z translator also allowed the grating box to be pulled completely out of the x-ray beam for telescope only measurements. The detector platform sat at the rear of the experiment chamber and held both the RGS Focal Camera (RFC) with its three CCDs and the Panter facility's Position Sensitive Proportional Counter (PSPC). The facility PSPC was similar to the one flown on the ROSAT satellite<sup>6</sup>. Mounted on the RFC's housing was a proportional counter used to cross-calibrate the RFC and the PSPC.

The RFC was mounted on z and x translators which allowed it to move from the MDM focus out to the Rowland circle position of the longest wavelength. The x translator had a range of  $\pm 200$  mm to allow measurement of a wide range of defocused positions. A y rotator allowed placement of the three CCDs tangent to the Rowland circle. A y translator allowed for height adjustment which was necessary for alignment and for changes in the spot height when taking measurements in and out of focus. A liquid nitrogen line ran through a chamber feedthrough to a cold block mounted on the detector platform. The cold block cooled the RFC via a braided copper strap.

The PSPC had a manipulator complement similar to the RFC's. The PSPC sat on the same z and x translators as the RFC so it was necessary to mount the PSPC on additional z and x translators to offset the RFC's motion. Positioning software checked to make sure there were no collisions between the RFC and the PSPC and limit switches provide physical protection.

During the course of the test it became evident that measurements of individual gratings within the box would be necessary. To accomplish this task, a slit mask with an opening just large enough to illuminate a single grating was

installed on a translator and positioned in front of the grating box. The mask translator's range was sufficient to allow for its complete removal.

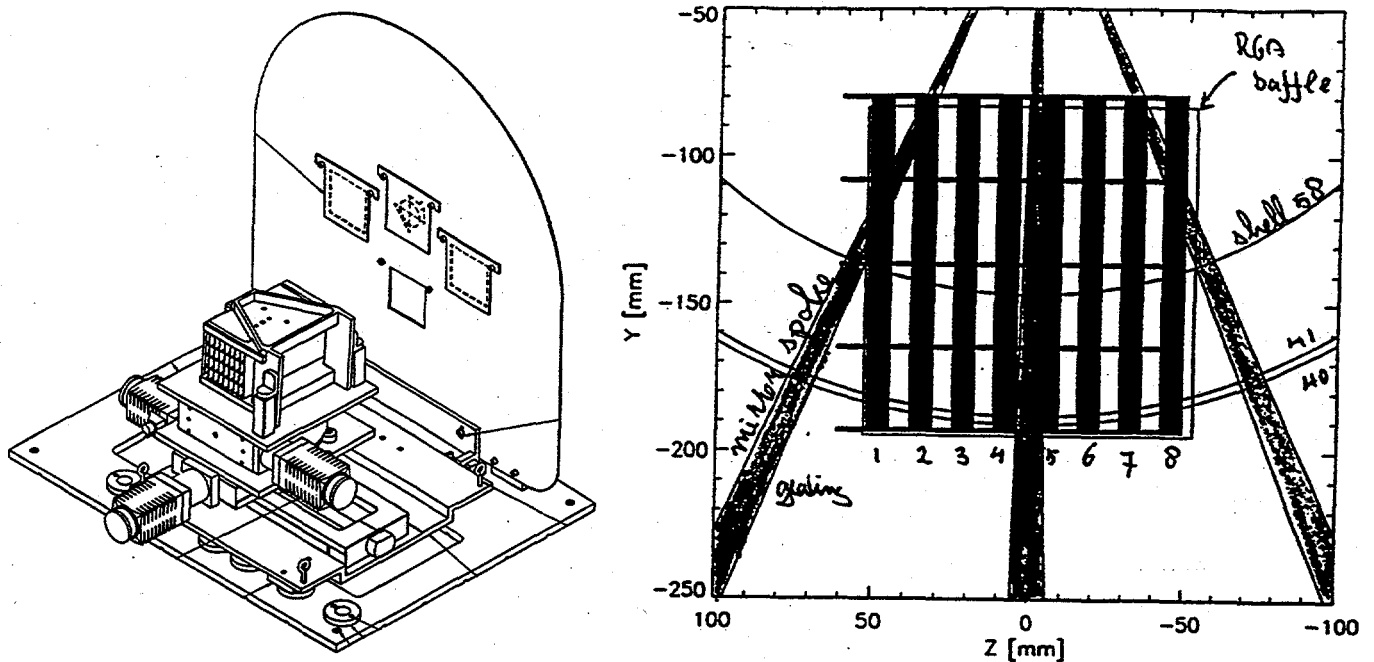


Figure 4. a.) Reflection Grating Array mounted on its x-z translators and y rotator. The box sits in the 6 o'clock position of the telescope mirror baffle. Openings for the 3 o'clock and unused 9 o'clock positions are to either side of the central baffle opening which was open during telescope alignment. b.) The projection of the grating box, mirror baffle, and mirror shells at the 6 o'clock position. In this position, each grating was illuminated along three narrow strips near the middle and edge.

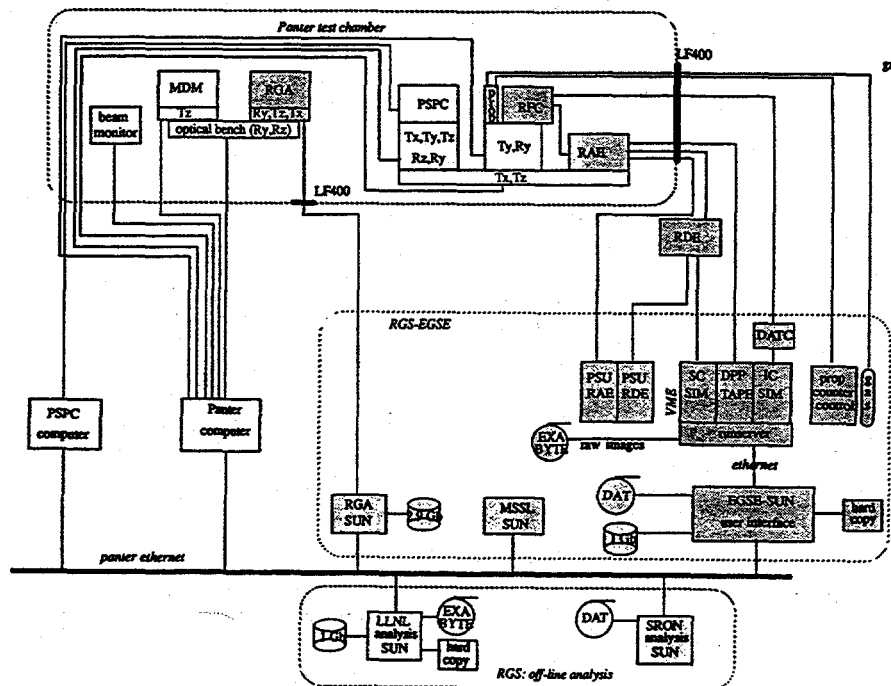


Figure 5. Computer hardware set up for control of the EOB testing.

A schematic picture of the computer control system is shown in Figure 5. Development of the overall system required the collaboration of several institutions. Five SUN Sparcstations were supplied by the experiment teams for instrument control and data analysis. The five computers were connected to each other and the world at large through an ethernet connection. In addition the Panter facility utilized a number of different computers for facility monitoring and control which were integrated into the overall system when possible.

#### 4. ALIGNMENT

Alignment tolerances were set by the future requirements of the flight instrument. The EOBB model with its large f number is much less sensitive to spot aberrations due to translational and rotational errors than the flight grating box. Through analytic and raytrace studies of the flight instrument, it was determined that the alignment procedure should insure relative placement of the grating box with respect to the MDM focus of  $\pm 0.5$  mm along the optical axis,  $\pm 1.0$  mm along the dispersion axis, and a grating box rotation within  $\pm 1$  arcminute for minimum optical aberrations. The alignment tolerances for the box as a unit are much more relaxed than those needed for individual gratings mounted within the box itself. Placement of the RFC and PSPC in x and z were held to  $\pm 1$  mm.

The alignment procedure relied on the use of a Leica TC2002 theodolite with attached infrared rangefinder to establish the proper location and orientation of each RGS element. A reference line was established by sighting through the viewport centered on the end of the experiment chamber down to the source. All subsequent alignments were made relative to this reference line.

After establishment of the reference line, rangefinder measurements were made to retroreflectors mounted on each object of interest. The differential distance measurements had an accuracy of 0.5 mm. Angular measurements to crosshairs mounted on the optics combined with the range information determined the distances perpendicular to the optical axis to within  $\pm 0.5$  mm also. Rotational positions were set by autocollimation off alignment mirrors and, in the case of the grating box, checked by autocollimation of the outermost grating which was visible through the side of the box after a rotation of slightly under ninety degrees. The perpendicularity of the RFC z translator to the defined optical axis was checked by positioning a pentaprism along the optical axis over the position of the translator. A needle was mounted on the translator and its cross motion monitored as it moved the translator's length.

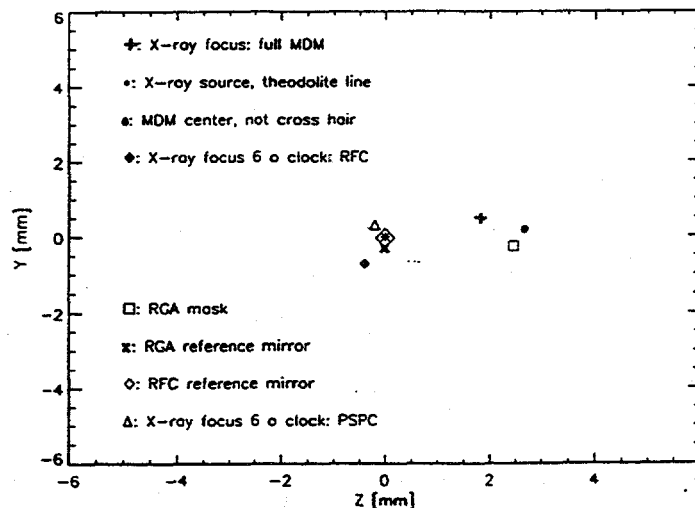


Figure 6. Final calculated position of source, telescope focus, and grating box.

The theodolite was mounted in a controlled area at the rear of the clean room adjoining the experiment chamber. Reference targets were positioned at several points in the room so that verification measurements could be taken during the eight weeks of testing to insure that the theodolite had not moved. Most alignment procedures were conducted with the experiment chamber at air and the rear chamber door open. Index of refraction corrections for measurements were negligible except for the calculation of the source distance.

During the alignment process, the translational and angular offsets of the alignment mirrors and crosshairs created a good deal of accounting difficulty before consistency was reached with the positioning of all of the fiducial points relative to one another. Figure 6 shows the final locations of the main optical components as calculated from the theodolite measurements. There remains a slight discrepancy between the full MDM focus and the focus from the 6 o'clock portion of the mirror which is believed to be an error in measuring the full MDM focal position.

The accuracy of the alignment was reflected in the measured position of the diffracted spots. Spot centroids were typically within 20 pixels (0.5 mm) of the expected location on the CCD. This implies a translational misalignment of ~0.3 mm or rotational misalignment of ~6 arcseconds if the grating box were totally responsible for the spot displacement.

## 5. TEST PROCEDURES

Primary experiment control was accomplished through the Electrical Ground Support Equipment (EGSE) program running on a Sparcstation. The EGSE controlled almost all aspects of the EOBB test. It initialized and verified the requested test geometry, monitored system housekeeping parameters before, during and after x-ray measurements, verified the status and performance of the instrument during testing, and inspected, logged, and archived the acquired detector and housekeeping data. Control flow was directed by menu selectable commands, execution of predefined procedures, or a combination of both. Experiment data was stored in real time to disk and archived onto tape on a regular basis. All data was entered into a database system for ease of later retrieval.

A typical measurement sequence began with the positioning of the optical components into the geometry specified for measurement. This geometry is dictated by the chosen source wavelength, diffraction order, position of the grating box relative to the MDM (3 or 6 o'clock), planned misalignments (defocus, decenter and tilt) of the grating box, source off-axis angle, defocus of the RFC, the CCD chosen for detection and the desired pixel on the CCD for the x-rays to hit. In addition, the PSPC was positioned to measure the MDM through beam. For those measurements where the grating slit mask was used, the position of the mask was set.

The source flux was adjusted for the changes in the optical system's efficiency with energy and order to yield an estimated count rate at the CCD of approximately  $5 \text{ s}^{-1}$ . This count rate, combined with the typical RGS spot sizes of about  $1 \text{ mm}^2$ , insured that double hits in individual pixels during a CCD readout cycle time of 3.73 seconds were not a problem. Before each x-ray measurement, a single full frame was collected. This full frame was subsequently used to set the threshold on the raw data and to correct for the background due to dark current and the residual light leaks inside the experiment chamber. The desired number of frames to be accumulated was entered into the EGSE and the measurement sequence initiated. The EGSE would first read out the position of all interface manipulators and other transducers and record them. It then initiated data collection with the desired CCD for the specified number of readout cycles. The EGSE had a real-time imaging display for a quick look at spatial and energy distributions. At a minimum this allowed verification that the detectors were in the correct position to detect the diffracted light.

Upon completion of the specified number of CCD readout cycles, the accumulated data were stored to disk. Near realtime image processing included background subtraction, split-event reconstruction and the formatting of the data into FITS files. For in-depth analysis of all data files (not only from the CCD, but also the PSPC, and the raytrace program) a image display and analysis program was developed. Using the FITS event files (typically x, y, and pulse height), images were assembled from events satisfying user defined pulse height constraints. Projections of this image onto the x- and y-axes were formed and plotted, and non-parametric statistics (median, sigma, skew, kurtosis, HEW) calculated for the distributions.

## 6. PRELIMINARY RESULTS

### 6.1 MDM

The MDM had been subjected to a series of measurements before the start of the EOBB to determine the imaging properties of the individual shells and the integrated telescope<sup>7</sup>. The MDM was removed from the test chamber after these initial tests and after reinstallation, the exact location of the focal point within the experiment chamber was not known. The location of the MDM focal point is critical to testing the grating box since it defines the origin of the coordinate system used to position the gratings and the detectors. It was therefore necessary to perform a series of measurements in and out of focus to establish the exact MDM focal position. Later range finding measurements of the distances to the focal point, the MDM position, and the source point showed the MDM focal length to be  $7499.3 \pm 0.5 \text{ mm}$  compared to the design focal length of  $7500.0 \text{ mm}$ .

Figure 7 shows the focal plane spot produced by the through beam at the 6 o'clock position. For this measurement the grating box by translated by half the grating-to-grating distance so that the light normally intercepted by the gratings passed through to the MDM focal plane. The hour glass shape is due to the preferential widening of the focused beam in the meridional plane due to scattering and figure errors. Blur in the sagittal plane is generally reduced by the sine of the incidence angle on the mirror. Each of the eight small sectors of light passing through the grating box forms a long thin focal line. This line is rotated at an angle which matches the azimuthal angle of the MDM sector that reflected the light. The MDM had a Half Energy Width (HEW) of 4 arcseconds at the 6 o'clock position.

## 6.2 RGS Resolution

One of the primary goals of the EOBB tests was to verify that the resolution of the integrated grating array was consistent with the performance predicted by pretest x-ray measurements of individual gratings and the metrology of the grating box performed during fabrication at LLNL.

The size of the diffracted spot for the RGS is composed of contributions from the telescope blur, the effects of replica nonflatness and scattering, and positioning errors of the replicas within the box. The magnitude of these effects are somewhat decreased with increasing diffraction order. The effect of the telescope's blur is reduced in the diffracted spot by  $\alpha/\beta \Delta\theta$ , where  $\Delta\theta$  is the telescope's angular blur and  $\alpha/\beta$  is the ratio of the incidence angle to the diffraction angle. Grating figure errors and rotational misplacement errors effect the spot width in the dispersion direction by  $(1+\alpha/\beta)\Delta\alpha$ , where  $\Delta\alpha$  is the change in incidence angle produced by these errors. For zero order,  $\alpha=\beta$  and the telescope blur contribution to the spot size is undiminished. In this case the spot size is determined by the full telescope blur and the grating box errors. For higher orders, the width of the diffracted spot decreases with respect to the zero order since the  $\beta$  angle increases.

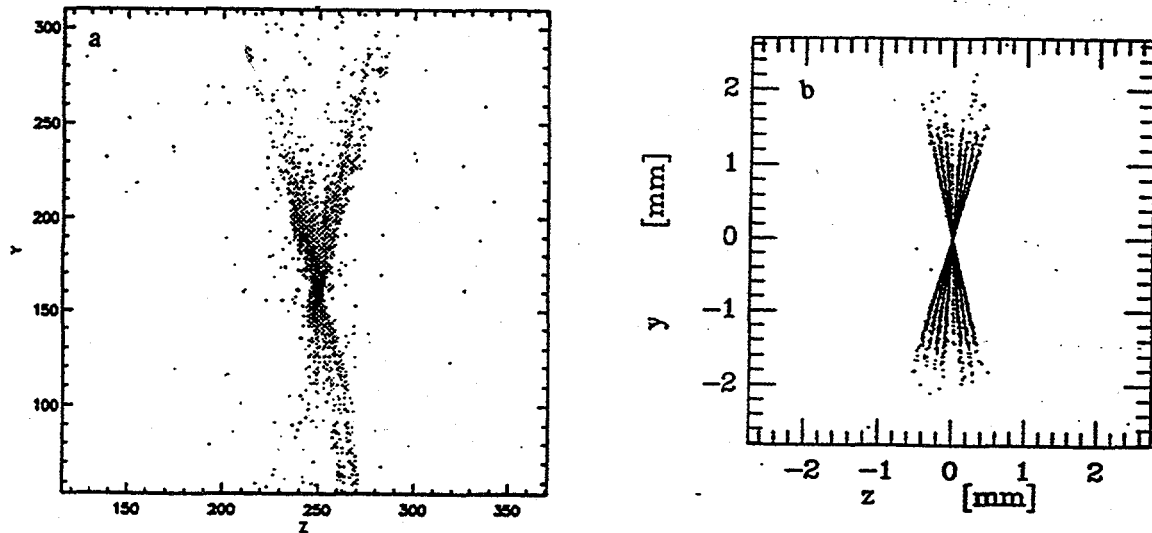


Figure 7 a.) Mirror response at the 6 o'clock position. Units are in pixels. b.) Raytraced spot pattern.

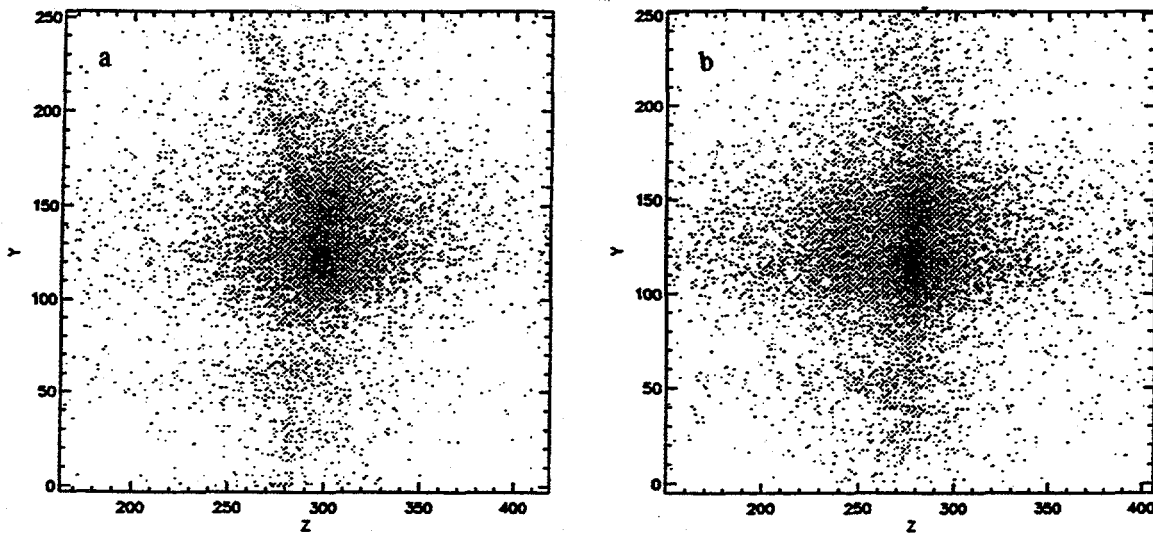


Figure 8. a.) The Mg K  $m=0$  spot measured with the full grating array. b.) The Mg K  $m=-2$  spot. Satellite lines are visible to the left of the central spot. Units are in pixels.

Pre-EOBB metrology of the grating box indicated that all of the mechanical tolerances with respect to individual grating figure and grating placement within the box had been met<sup>5</sup>. The expected contribution to the spot size from mechanical errors was at the level of a few arcseconds. Grating placement errors within the box were expected to contribute 3.8 arcseconds to the zero order spot size. Grating figure measurements indicated a two arcsecond contribution to spot size. Pre-EOBB X-ray resolution measurements were performed on the master grating and optical tests were performed to verify its correct line space variation. These measurements indicated a few arcsecond contribution to the resolution from the grating itself. Unfortunately, time constraints did not permit a full characterization of the resolution properties of the individual replica gratings before the EOBB tests.

The MDM beam at the 6 o'clock position had a measured HEW of 4 arcseconds. With the telescope beam size larger than all other spot size contributions, only a modest increase for the zero order Mg K spot was expected. It was therefore surprising when the Mg K zero order beam, shown in Figure 8, was found to have a HEW of 20 arcseconds, several times wider than the through beam. To investigate the cause of the widening, a slit mask, described in Section 3.1, was inserted between the MDM and the grating box to allow the study of the spot profile from each of the eight gratings. These measurements of the individual gratings revealed that seven of the eight replicas had profiles ranging from 15 to 18 arcseconds HEW, appreciably greater than the HEW of the illuminating MDM beam. Grating #8 had somewhat better performance than the other seven with a HEW of 7 arcseconds.

Even with the anomalously broad line profiles from the individual gratings, it was still possible to verify the mechanical accuracy of the placement of the gratings. Measurements of the Mg K  $m=0$  and  $m=-2$  spots were obtained for each individual grating by sequentially moving the slit mask without moving any other part of the optical system. Figure 9 shows the measured deviation of the  $m=0$  and  $m=-2$  spot centroid for each of the eight gratings. The measured rms spot deviation of 3.2 arcseconds for the zero order spot is well within the specified tolerance for the grating box.

The cause of the line broadening was further investigated by measuring the HEW of the line profile as a function of incidence angle, energy, and order<sup>8</sup>. This analysis confirmed that the grating's figure was not the cause of the widening. With fabrication errors and grating figure errors eliminated, the most likely explanation for the line broadening was scattering due to surface roughness. Post-EOBB tests, discussed in the last section, confirmed this diagnosis.

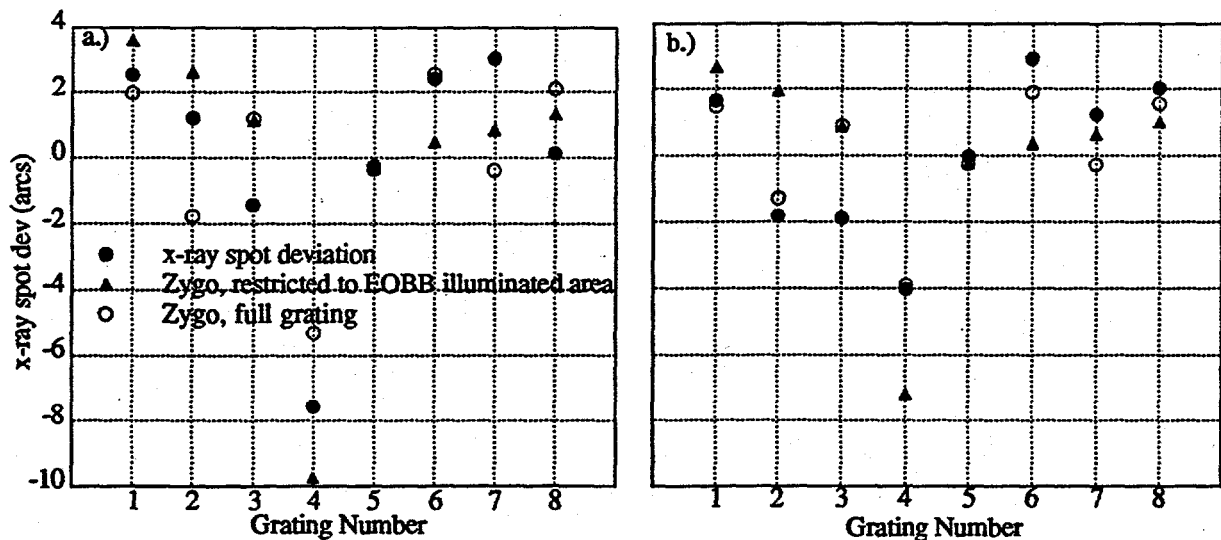


Figure 9. Deviation of the a.) Mg K  $m=0$  and b.) Mg K  $m=-2$  spot measured for each of the eight gratings in the EOBB grating box. Also shown are the predicted deviations based on post-EOBB measurements of the grating-to-grating alignment.

### 6.3 Grating Array Obscuration

The grating box blocks light from reaching the focal plane. To verify that the actual obscuration matched the geometric projection of the mirror shells onto the grating box (see Figure 4b), measurements of the focal plane countrate were taken with the grating box in and out of the telescope beam. For the EOBB 6 o'clock configuration it was calculated that 57.5 percent of the light would be intercepted by the gratings or blocked by the box. The ratio of the box in to box out fluxes gave a measured ratio of 56.9 percent.

The effect of the grating box on the EPIC on-axis point spread function was also measured in the 6 o'clock position and is shown in Figure 10. A small shift in the peak of the distribution is seen, probably due to the slightly asymmetric blockage of the MDM beam by the gratings, which were offset from the centerline of the beam (visible in Figure 4b).

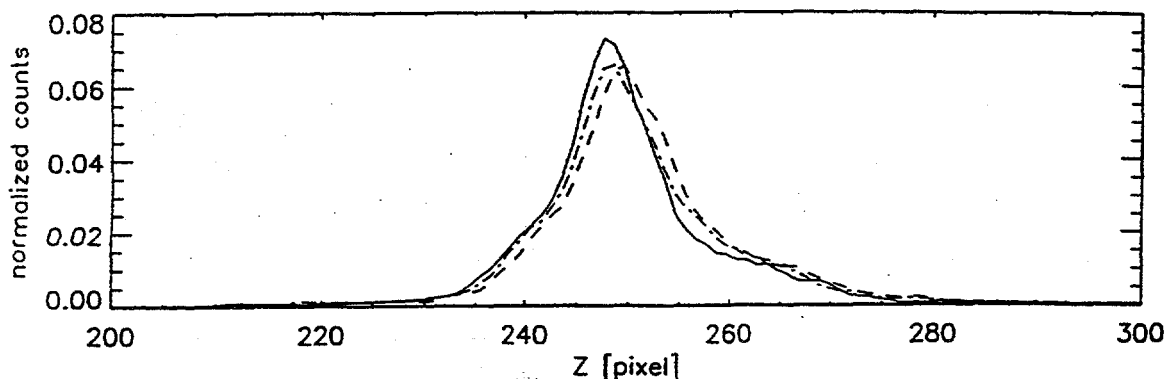


Figure 10. EPIC point spread function with (dashed and dashed/dotted) and without (solid) the grating box in place.

## 7. POST-EOBB GRATING BOX TESTS

To verify the pre-EOBB metrology and to help pinpoint the cause of the wide line profiles, a series of measurements were performed as part of the post-EOBB analysis of the RGA grating box. The grating figures were examined for conformance with the flatness tolerance. The grating-to-grating angular variation was checked. After removal from the grating box, a close visual examination of grating surfaces was performed under a variety of lighting conditions. Finally, the grating surface properties were measured using optical microscopes and two ZYGO interferometers.

### 7.1 Grating Figure and Alignment Measurements

Measurements of the grating figure were made using a ZYGO Mark IV interferometer during RGA box disassembly. The grating surfaces were extremely flat in the dispersion direction with an rms surface slope of 1.1 arcseconds, equal to the pre-EOBB measurement. However, it was evident from comparison of the pre- and post-EOBB grating surface contours that a systematic twist of about 1.5 waves had developed in all of the gratings. With the inclusion of this twist the grating rms slope equaled 1.9 arcseconds. Either way, these slope distributions are still within the specified fabrication tolerance for combined grating figure and twist and well below a level that could contribute to the line broadening seen in the individual gratings. It was determined that the twist was due to movement in the Invar box structure, which used a nonflight material and design.

During the disassembly process, the RGA was mounted on a precision rotator containing an interferometric angular readout calibrated to 0.2 arcseconds. As each grating was removed from the box, the rotator was moved by 352 arcseconds, the design grating-to-grating angle. After the rotation, a ZYGO measurement of the next grating's figure was made. The mean of the slope distribution from the ZYGO measurement gives the tilt error of the grating's surface. The results of these measurements are plotted in Figure 9 as the x-ray spot deviations that should result from the measured grating tilts. The rms angular deviations of the gratings needed to produce the measured x-ray spot deviations is 1.9 arcseconds, within the fabrication tolerance.

As Figure 9 shows, the spot deviations predicted from the ZYGO measurements and the x-ray measured deviations are fairly well correlated. The x-ray spot motion is not expected to track the ZYGO data exactly since grating tilt/twist is only one of several mechanical alignments that effect the x-ray spot position. Grating translation errors in both z and x can play a significant role in the x-ray spot's median position.

From the analysis of the x-ray spot measurements and the ZYGO interferometer data we conclude that the contribution of the translational, rotational, and twist errors to the measured x-ray spot size was within the specified tolerances and were not the cause of the broad line profile seen in Figure 8.

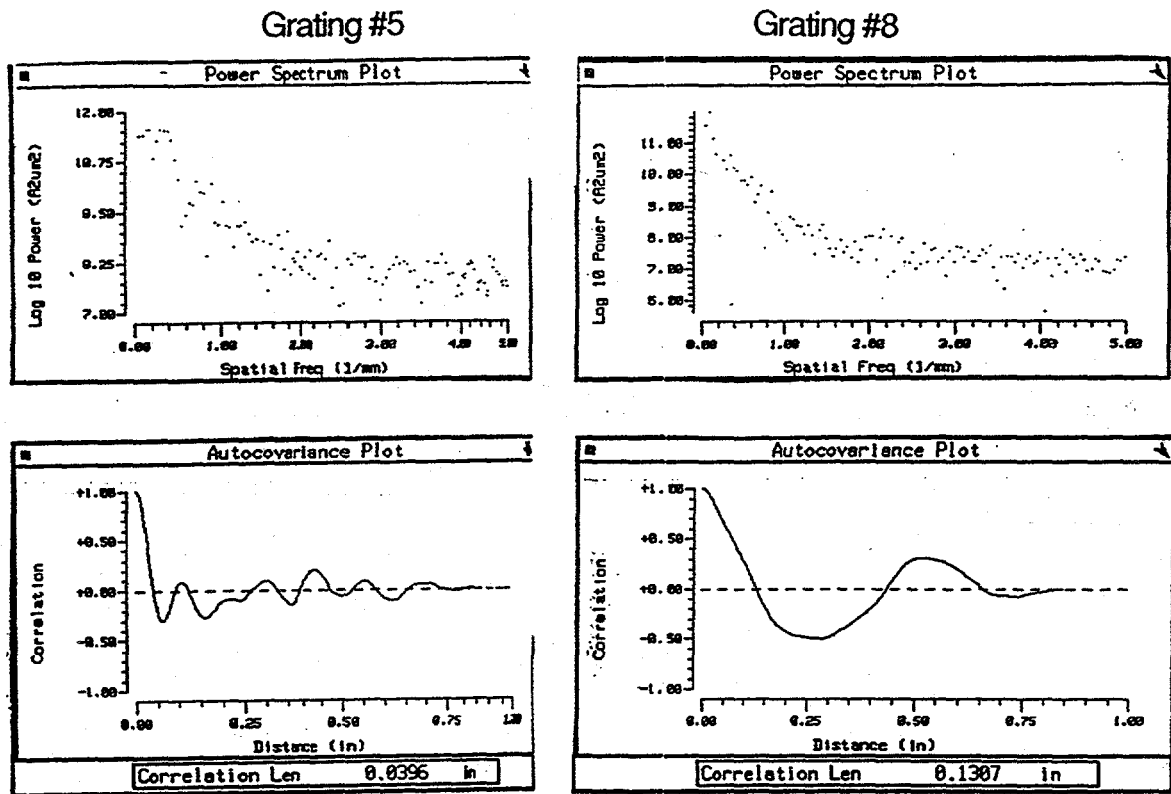


Figure 11. Power spectral density and autocovariance functions derived from ZYGO metrology of gratings #5 and #8. Grating #5 is the worst of the seven high scattering gratings in the RGS. Grating #8 exhibits less power at all surface scattering frequencies and has a significantly larger correlation length than grating #5.

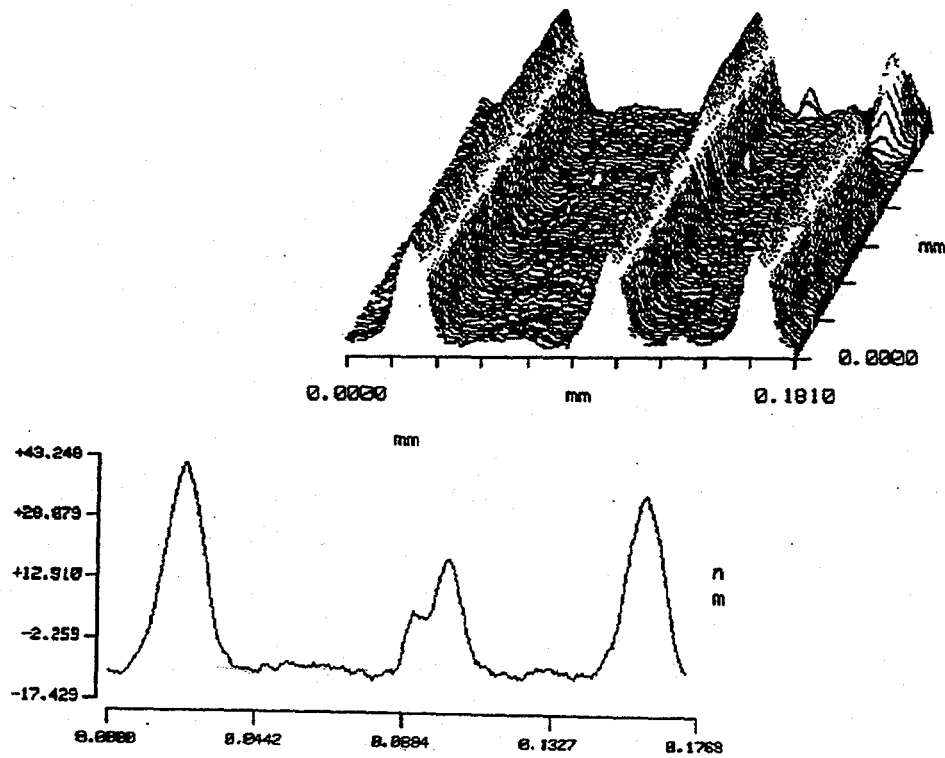


Figure 12. Surface profile of grating #5 using a ZYGO Mark III interferometer at 40x. The profile shows the cross section of the ridge like features that produce the crazing observed visually. The lateral scale of the features is consistent with the observed x-ray scattering profile widths.

## 7.2 Visual and Microscopic Inspection of the Replicas

Close visual inspection under controlled lighting of the grating surfaces revealed a subtle 'crazed' appearance except for grating #8 which had substantially less of the effect. Three replicas not mounted in the RGA box and which had been stored untouched in a dry box also showed the effect. Optics from replication study phases leading up to the EOBB replication did not show this effect. These optics include full sized mirrors replicated onto glass and SiC substrates of stiffness equal to the EOBB substrates and small 38 mm square gratings on glass substrates which had been used in studies of efficiency loss with multi-generational replication.

Microscopic examination of the replica surfaces confirmed the existence of ridge like structures running mainly in a direction parallel to the grooves. Ridges running non-parallel to the grooves could be observed close to the replica edges.

The individual gratings were examined under 6x magnification using the ZYGO interferometer. Differences between the lower scattering grating #8 and the other gratings are clearly evident in the Power Spectral Densities shown in Figure 11. Grating #8 shows less power at all surface frequencies and particularly below  $1 \text{ mm}^{-1}$ . The visual impression of larger scale features on grating #8 is confirmed in the longer correlation length of its autocorrelation function also plotted in Figure 11. The use of similar ZYGO measurements for future grating replicas will be an important quality control tool for determining replica acceptance.

Figure 12 shows a surface profile of grating #5 under 40x magnification using a ZYGO Mark III interferometer. The crazing of the gratings surface is dramatically illustrated (grating #5 had the qualitatively worst looking surface). The surface features exhibit the 100-200 micron length scales necessary to explain the observed x-ray scattering profiles.

The origin of the surface crazing is most probably due to separation stresses inherent in the replication process. The force of separation between the master and replica can be much larger with gratings than with mirrors. We are working with the grating vendor to produce a replication process which minimizes separation stresses.

### Acknowledgments

Many people have contributed to these tests and we would like to thank the technical staffs from all of the participating institutions. This work was performed in part under the auspices of the U.S. Department of Energy by the Lawrence Livermore National Laboratory under contract #W-7405-ENG-48.

### References

1. P. Barr, J. Bergeron, J. Bleeker, J. Ellwood, A. Gabriel, P. Giommi, R. Mushotzky, R. Pallavicini, J. van Paradijs, A. Peacock, K. Pounds, H. Schnopper, B.G. Taylor, J. Trumper, G. Whitcomb, N. White, "The High-Throughput X-ray Spectroscopy Mission", ed. B. Battrick, ESA SP-1097, European Space Agency, Paris, 1988.
2. O. Citterio, P. Conconi, M. Ghigo, F. Mazzoleni, H. Brauningner, W. Burkert, N. Schulz, P. Gondoin, K. van Katwijk, R. Laurance, "Results on electroformed mirror shells for the XMM project", SPIE Proc. 1742, 256, 1992.
3. J.V. Bixler, C.J. Hailey, C.W. Mauche, P.F. Teague, R.S. Thoe, S.M. Kahn, and F.B.S. Paerels, "Performance of a variable line spaced master reflection grating for use in the Reflection Grating Spectrometer of the X-ray Multimirror Mission", SPIE Proc. 1549, 420, 1991.
4. J.V. Bixler et al., in preparation.
5. T.A. Decker, R. Montesanti, J.V. Bixler, C.J. Hailey, S.M. Kahn, "Development, fabrication and metrology of the Electro-Optical Breadboard Model for the Reflection Grating Array of the XMM grating spectrometer", accepted for publication in SPIE Proc. 2283, 1994.
6. F. Pfeifferman et al., SPIE Proc. 733, 519, 1987.
7. P. Gondoin, K. van Katwijk, "XMM telescope", accepted for publication in SPIE Proc. 2279, 1994.
8. S.M. Kahn, J.V. Bixler, C.J. Hailey, C.W. Mauche, F.B.S. Paerels, J.W. den Herder, "Modeling and analysis of x-ray emission line images acquired with a prototype model of the XMM Reflection Grating Spectrometer", accepted for publication in SPIE Proc. 2283, 1994.